



## Numerical Modeling of a Dielectric Discharge Plasma Actuator Using Local Energy Approximation for Application to Flow Control

Moustapha Ouali\*<sup>ORCID</sup>, Youssef Lagmich<sup>ORCID</sup>

Department of Physics, Laboratory of Sciences and Advanced Technologies, Polydisciplinary Faculty of Larache, Abdelmalek Essaadi University, Tetouan 93030, Morocco

Corresponding Author Email: [moustaphaouali@gmail.com](mailto:moustaphaouali@gmail.com)

Copyright: ©2024 The authors. This article is published by IIETA and is licensed under the CC BY 4.0 license (<http://creativecommons.org/licenses/by/4.0/>).

<https://doi.org/10.18280/mmep.110709>

### ABSTRACT

**Received:** 5 January 2024  
**Revised:** 17 April 2024  
**Accepted:** 25 April 2024  
**Available online:** 31 July 2024

#### Keywords:

*dielectric barrier discharge plasma actuator, dielectric barrier discharge, flow control, parametric analysis, ion velocity, relative permittivity*

The primary benefit of the DBD plasma actuator is its macroscopic stability, which makes it one of the most frequently cited plasma actuators in the academic literature. This study examined the potential of dielectric barrier discharge (DBD) plasma actuators for flow control. The plasma actuator is composed of an exposed electrode, a covered electrode, and a dielectric layer that separates the electrodes. A parametric analysis was performed to explore the impact of macroscopic variables, such as pressure, applied voltage, and relative permittivity of the dielectric, on the transfer of momentum between particles affected by Coulomb forces. The results underscore the crucial influence of the dielectric material on ion velocity. The observed trend demonstrates a clear connection between the increase in the relative permittivity of the dielectric material and the corresponding increase in ion velocity. This emphasises the significant importance of choosing the correct dielectric material, particularly in situations where ion velocity is critical, such as in the precise regulation of airflow around an aerodynamic profile.

## 1. INTRODUCTION

Since the inception of the first aircraft, humanity has consistently sought to enhance the performance and efficiency of these systems, all in pursuit of achieving a more seamless and comfortable flying experience, regardless of prevailing weather conditions. Our research aligns with this objective as we delve into the incorporation of cold plasma technology generated by dielectric barrier discharge (DBD) and its implications in the field of aerodynamics.

The concept of a "plasma" actuator revolves around the creation of a cold plasma at the surface of an obstacle to modify the flow properties as shown in Figure 1. This actuator, generally established at atmospheric pressure, uses an electrical discharge between two electrodes positioned at the edge of the profile in Figure 2, resulting in the generation of tangential ionic wind at the wall of the aerodynamic profile. This plasma jet has applications in airflow control, such as aircraft wings or wind turbine blades, reducing drag, increasing lift and improving aerodynamic efficiency [1-8]. Plasma actuators with a surface dielectric barrier discharge (DBD) offer several advantages for flow control [9]. They are designed to be non-intrusive, allowing precise flow control close to surfaces without causing physical contact, promoting energy efficiency, low power consumption and cost effectiveness [10-13]. In addition, their fast response time facilitates rapid and accurate flow adjustments when changes are detected [14, 15], while attenuating noise and vibration, particularly crucial in aerospace applications for passenger comfort and safety. These advantages make DBD plasma actuators an attractive choice for a variety of flow control applications. Nevertheless, further research is needed to improve flow control [16], as current manufacturing methods limit their performance and wider applicability [17]. Recent optimizations, incorporating improved choices of thick dielectric materials and AC input frequencies and waveforms, have led to substantial performance improvements over previous designs [18].

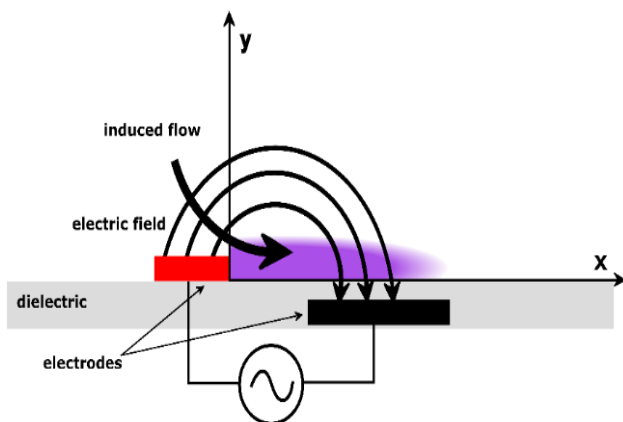


**Figure 1.** Schematic diagram of ion wind generation for a surface DBD

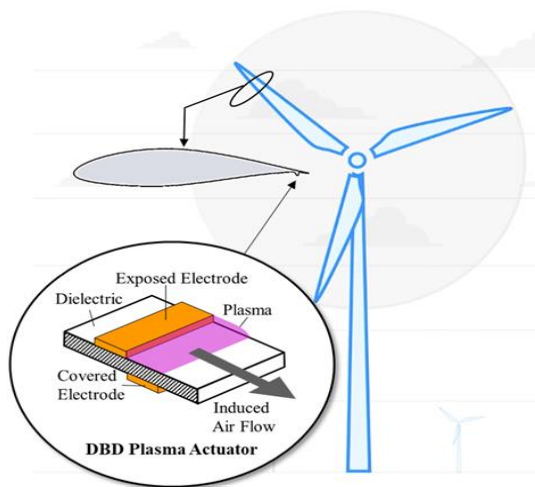


**Figure 2.** Schematic active aerodynamic load control for wind turbines [19]

In this study, we examined the influence of dielectric properties on the transmission of an electric field within the plasma. We focused on two key characteristics of dielectric materials: permittivity and the secondary electron emission coefficient. Permittivity is the ability of a material to store electrical energy in the presence of an electric field. In plasma, permittivity plays a fundamental role in the propagation of the electric field through the medium. Higher permittivity values indicate that the material has a better ability to store electrical energy, resulting in a more extensive and efficient propagation of the electric field within the plasma. The secondary electron emission coefficient refers to the ability of a material to release electrons when subjected to energetic particles. In the field of plasma, this attribute becomes increasingly important because it can increase the electric current needed to propagate the plasma. A high secondary electron emission coefficient means that the material is more efficient at emitting electrons, thereby helping to power and fortify the plasma. In essence, the scientific study confirmed that permittivity and secondary electron emission coefficient are essential characteristics of dielectric materials that can influence the transmission of electric fields within the plasma. By understanding and manipulating these properties, researchers can design more efficient plasma systems suitable for a wide range of applications.

## 2. CLOSED-LOOP CONTROL OF AIRFLOW AROUND WIND TURBINE BLADES OR AIRCRAFT WINGS USING DBD PLASMA FOR IMPROVED PERFORMANCE

Closed-loop control of airflow around wind turbine blades or aircraft wings using dielectric barrier discharge (DBD) plasma is a technique that involves using closed-loop control to manipulate airflow and improve the performance of the system. A DBD surface discharge generates no thermal plasma, allowing modification of the boundary layer of the airflow [20].

The principal aim of this technique is to attain a stable and controllable airflow, which is essential for various applications, including power generation, transportation and aerospace engineering. In a closed-loop control system that regulates the airflow using DBD plasma, sensors measure critical airflow parameters, such as velocity, pressure and turbulence. This

data is then conveyed to the controller, which adjusts the plasma input to effectively alter the airflow. The closed-loop control system persistently monitors the airflow and adjusts the plasma inlet in real-time where necessary to maintain the desired airflow conditions. This approach not only permits precise and stable control of airflow, but also has the potential to enhance performance, for instance, by increasing lift, diminishing drag and augmenting fuel efficiency.

Furthermore, the system can be optimised for varying operating conditions and environmental factors by adjusting the airflow to meet the desired performance objectives. This ultimately contributes significantly to reducing system variability, thereby improving safety and reliability. Further research and development efforts are required to comprehensively investigate the feasible applications of this technology within the domains of wind turbine blades or aircraft wings [21].

## 3. NUMERICAL STUDY OF DIELECTRIC BARRIER DISCHARGE IN PURE OXYGEN AT ATMOSPHERIC PRESSURE

In the context of our study, we have opted to employ the fluid model to elucidate plasma dynamics. This decision arises from our research focus on macroscopic observables, eschewing microscopic intricacies. We are particularly interested in quantifiable parameters such as average velocity, energy, and density of the plasma. Consequently, we have embraced the fluid model to conceptualize the plasma as a charged fluid due to its simplicity and alignment with our research goals. This choice is driven by the fluid model's ability to effectively capture macroscopic phenomena, offering results directly applicable to experimental measurements. Unlike kinetic or particle-based models, which demand a deeper understanding of microscopic interactions, the fluid model offers a more intuitive and accessible approach tailored to our study. It is imperative to underscore that the selection of the model hinges on the specific nature of our investigation. In our case, the fluid model emerges as the most apt for dissecting plasma behavior within a dielectric barrier discharge in an oxygen-rich environment. By prioritizing macroscopic and measurable parameters, our simulation promises insights into discharge characteristics, fostering optimization for diverse practical applications control for wind turbines for example.

In line with our research methodology, we have developed a two-dimensional numerical simulation model tailored to investigate the behavior of the dielectric barrier discharge within an oxygen-rich environment. Using three fluid equations derived from the Boltzmann equation, this model seeks to analyze the impact of key variables such as the relative permittivity of the dielectric barrier, and the amplitude and frequency of the applied voltage on the performance of the discharge at atmospheric pressure. This simulation focuses on the macroscopic aspects of the discharge, such as density, average velocity and average energy, while highlighting the physical characteristics of the discharge, enabling its use in a variety of practical applications to be optimized.

### 3.1 Limitations of the local field approximation for plasma modeling

This passage discusses the Local Field Approximation

(LFA), a simplifying assumption used in plasma modeling that assumes Townsend coefficients and electron mobility are only functions of the local reduced electric field [22]. The LFA approach is not always justified for electrons [23] because it assumes there is no energy transport other than by collisional processes. Instead, solving the electron energy transport equation and determining the electron mobility, diffusion coefficient, and reaction rates from the average electron energy ( $\bar{\varepsilon}$ ) can provide a better representation of the driving force and allow for non-local effects through convection and diffusion of electron energy [24, 25].

### 3.2 The Local Energy Approximation fluid model for cold plasma without thermal equilibrium local

The Local Energy Approximation (LEA) fluid model for cold plasma without Local Thermal Equilibrium (LTE) assumption is a more complex version of the LEA model that takes into account the non-equilibrium nature of plasma.

The LEA fluid model without LTE assumption describes the plasma using the following equations:

$$\frac{\partial n_k}{\partial t} + \nabla(\Gamma_k) = S_k \quad (1)$$

The continuity Eq. (1) can be used to represent the variation rates of the density of charged species, where  $n_k$  is the volume mass,  $S_k$  is the source term that depends on the ionization and  $\Gamma_k$  is the k-particle flux (k=e, i refers to electrons and positive ions).

$$\frac{\partial(n_e m_e u_e)}{\partial t} + \nabla \cdot n_e m_e u_e = -(\nabla \cdot p_e) + q n_e E - n_e m_e u_e \nu_m \quad (2)$$

The rate of variation of the electron momentum is described by Eq. (2): Where  $m_e$  is the electron mass,  $p_e$  is the electron pressure tensor,  $u_e$  is the electron drift velocity, E is the electric field,  $q$  is the electron charge and  $\nu_m$  is the momentum transfer frequency.

To determine the flux term in Eq. (2), a simplification method called the drift-diffusion approximation is applied instead of explicitly solving the first moment of the Boltzmann equation. When the ionization and attachment frequencies, along with the angular frequency, are significantly lower than the angular momentum transfer frequency, the first term on the left side of Eq. (2) it acceptable to ignore. Alternatively, one can omit the second term in Eq. (2) by assuming that the electron drift velocity is less than the thermal velocity. For cases following a Maxwell-Boltzmann distribution, the pressure term, denoted as  $p_e$ , expression (3) can be used in its place, where  $I$  represents the identity matrix, and  $T_e$  stands for the electron temperature.

$$p_e = n_e k_B T_e I \quad (3)$$

Finally, Eq. (4) provides the charged particle flux with  $\mu_k$ ,  $D_k$  and  $E$  are the mobility of charged species, the diffusion coefficient and the electric field respectively.

$$\Gamma_k = n_k u_k = B \cdot (n_k \mu_k E - \nabla n_k D_k) \quad (4)$$

$$B = \begin{cases} -1 & \text{for electrons} \\ +1 & \text{for ions} \end{cases}$$

The energy conservation Eq. (5) is exploited to establish the final expression for the electron energy density, including the

drift-diffusion approximation. with  $\varepsilon$  the mean electron energy,  $S_e$  the energy of the electrons lost by collisions,  $\Gamma_e$  the mean electron flux energy,  $\mu_e$  the electron mobility and  $D_e$  the electron flux diffusion coefficient.

$$\frac{\partial(n_e \varepsilon)}{\partial t} + \nabla(\Gamma_e) + E \cdot \Gamma_e = S_e \quad (5)$$

$$\Gamma_e = -n_e \mu_e E - \nabla \cdot D_e \quad (6)$$

The fluid equations, where  $V$  is the electrostatic potential,  $\varepsilon_0$  is the space permittivity and  $q$  is the electron charge, are used to determine the electric field using Poisson's Eq. (8).

$$\Delta V = \frac{q}{\varepsilon_0} (n_e - n_i) \quad (7)$$

$$E = -\nabla V \quad (8)$$

### 3.3 Boundary conditions

Secondary emission effects, resulting in electron accumulation and random motion within a short distance from the surface, typically within a few mean free paths, influence the behavior of electron flow near boundaries. This phenomenon is described mathematically by Eq. (9), which accounts for electron gain, and Eq. (10), which governs the flux of electron energy. Eq. (9) further elaborates on this by depicting the gain of electrons due to secondary emission effects, quantified by the secondary emission coefficient, denoted as  $\gamma_i$ .

$$n \cdot \Gamma_e = \left( \frac{1}{2} v_{e,th} n_e \right) - \left[ \sum_i \gamma_i (\Gamma_i \cdot n) \right] \quad (9)$$

The secondary emission energy flux, as described in Eq. (10), is represented by the second term,  $\varphi_i$ , indicating the average energy of secondary electrons. This term accounts for the transfer of energy carried by secondary electrons. Additionally, for heavier species, interactions at the surface result in the loss of ions directed towards the wall. This phenomenon occurs due to the electric field orientation, which guides the movement of ions towards the wall. Furthermore, the surface interactions play a crucial role in altering the trajectories of ions and electrons, contributing significantly to the overall dynamics near boundaries.

$$n \cdot \Gamma_e = \left( \frac{5}{6} v_{e,th} n_e \right) - \left[ \sum_i \gamma_i \varphi_i (\Gamma_i \cdot n) \right] \quad (10)$$

Similarly, the described boundary condition arises due to the aggregation of charges at the interface of the dielectric surface, with  $\varepsilon_1$  and  $\varepsilon_2$  representing the relative permittivities of the gas and the dielectric material, respectively. This condition underscores the significance of charge accumulation at the dielectric interface in influencing the electric field distribution and subsequent phenomena within the system. Such concentration of charges can profoundly affect the dynamics of plasma actuators, influencing factors such as ionization rates, electron mobility, and overall device performance. Understanding and properly accounting for these boundary conditions are essential for accurate modeling and optimization of plasma-based technologies in various

applications, including aerodynamics, energy systems, and materials processing.

$$n \cdot (D_1 - D_2) = \rho \tag{11}$$

$$n \cdot (E_1 \varepsilon_1 - E_2 \varepsilon_2) = \rho \tag{12}$$

where,  $D_1$  and  $D_2$  denote the displacement electric fields within and outside the dielectric tube, respectively. The displacement field, often represented by  $D$ , is a fundamental concept in electromagnetism, describing the ability of a material to polarize under the influence of an electric field. The displacement field reflects the response of the material to the applied electric field, providing insights into its dielectric properties. The surface charge density,  $\rho_s$ , arises from the polarization of charges on the dielectric surface due to the electric field. By solving the equation governing the surface charge density, one can obtain valuable information about the behavior of charges at the dielectric interface. This understanding is crucial for characterizing the interaction between the dielectric material and the surrounding medium, guiding the design and optimization of devices such as plasma actuators, capacitors, and dielectric barriers.

$$\frac{d\rho_s}{dt} = n \cdot J_i + n \cdot J_e \tag{13}$$

The normal component of the total ion current density at the wall is denoted as  $n \cdot J_i$ , where  $n$  represents the normal vector to the surface, and  $J_i$  signifies the ion current density. Similarly, the normal component of the total electron current density at the wall is represented by  $n \cdot J_e$ , where  $J_e$  symbolizes the electron current density. These expressions quantify the flux of ions and electrons perpendicular to the surface, providing essential information about the transport of charged particles near boundaries. Understanding these components is crucial for analyzing the behavior of plasma near surfaces, guiding the development of plasma-based technologies in various applications, including aerospace, materials processing, and energy systems.

The simultaneous solution of these equations is achievable through the finite element method within the COMSOL Multiphysics software, facilitating the acquisition of a self-consistent solution for plasma behavior. This includes an analysis of local energy deposition and transfer processes. The Local Energy Approximation (LEA) method, a computationally efficient approach, offers valuable insights into the intricate and nonlinear dynamics of plasmas. Through the LEA method, researchers can gain a deeper understanding of how energy is distributed and transferred within the plasma, enhancing our comprehension of plasma physics phenomena and supporting the development of advanced plasma-based technologies.

#### 4. RESULTS AND DISCUSSION

This series of simulations embarked on a fundamental inquiry aimed at discerning the parameters amenable to modification for altering the characteristics of the plasma actuator. Key factors investigated included electron and ion density, ionization rate, electric field, and deposited energy. Additionally, we aimed to elucidate the potential impact of dielectric permittivity on the velocity of the ionic wind within the surface plasma actuator. Through meticulous simulations,

we unveiled the spatio-temporal variation in various parameters, providing a comprehensive insight into the dynamic behavior of the system. Notably, we implemented several simplifications and adjustments to facilitate the simulations, such as considering a single ionic species and neglecting excited states, while accounting only for ionizing collisions in our modeling approach. These adjustments were necessary to address the intricacies of the numerical problem while ensuring computational tractability.

Given the intricacies of the numerical problem, several simplifications and adjustments were necessary to facilitate the simulations. For instance, we limited our consideration to a single ionic species, neglecting the contribution of excited states. Additionally, only ionizing collisions were accounted for in our modeling approach. The applied sinusoidal voltage,  $V(t)=10 \text{ kV} \sin(2\pi f)$ , with a frequency of 1 kHz, served as the driving force for the simulations. At the outset, an initial density of electrons and ions ( $n_{e,0} = n_{i,0} = 10^8 \text{ cm}^{-3}$ ) permeated the domain, initiating the discharge with an initial electron energy of 5V. Other key parameters included an electron emission coefficient by the dielectric material of order 0.02 and a secondary electron energy of 2.5V. Throughout the simulations, a discharge temperature of 300K and atmospheric pressure were assumed as standard conditions.

Utilizing a numerical modeling approach, we tackled our system of equations employing the COMSOL Multiphysics software coupled with the finite element method. To accurately represent our domain, we discretized it into unit cells, as illustrated in Figure 3. The mesh, comprising 51504 units of a free triangular type, was meticulously crafted to capture the intricacies of fluid interaction and dielectric material regions. Our emphasis on refining the mesh in these critical areas underscores our commitment to dissecting the particle interactions integral to our study. This focused approach facilitates a nuanced analysis of the influential interactions, thereby enriching our understanding of the underlying dynamics.

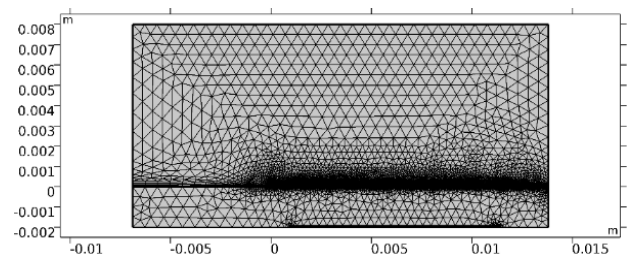


Figure 3. Computational geometry domain

#### 4.1 Confrontation of experimental and numerical results

The investigation of ionic motion in surface dielectric barrier discharge (DBD) systems is crucial for aerodynamic flow control optimization, especially for aerodynamic profile performance. A significant aspect of this study is comprehending the effect of the dielectric constant on ion behavior near the surface. The dielectric constant has a direct impact on the electric field distribution within the DBD configuration, which affects the acceleration and trajectory of ions. Researchers can develop advanced strategies for manipulating airflow over aerodynamic surfaces by comprehensively exploring how variations in the dielectric constant affect the velocity profile of ions near the surface. This nuanced understanding facilitates precise control of boundary layer characteristics, allowing for the mitigation of

flow separation, postponement of stall onset, and enhancement of overall aerodynamic efficiency. The study of the dielectric constant in surface DBD systems holds immense promise for advancing aerodynamic flow control techniques and optimizing the performance of various aerospace and automotive applications.

To further strengthen the validation of our model, we meticulously compared our findings against a broad spectrum of sources, including published literature and experimental studies [26-28]. This comprehensive approach aimed to ensure the robustness and credibility of our results within the established scientific discourse. Our particular emphasis was on scrutinizing the velocity profile across varying altitudes, specifically considering a dielectric constant of 2.5. This rigorous validation process not only underscores the accuracy of our model but also enriches the broader understanding of ion dynamics in surface DBD systems.

The outcomes of our analysis revealed a congruence with the velocity profile reported in the existing literature, particularly in proximity to the dielectric material, where a maximum velocity of 3.5 m/s was attained at a distance of 12 mm from the exposed electrode as shown in Figure 4. These results were obtained under the conditions of a sinusoidal AC voltage with an amplitude of 10 kV with a frequency of 1 kHz and it is crucial to note that the instant  $t=250 \mu\text{s}$  corresponds to the peak of the first half-cycle of the applied voltage with a maximum amplitude. Additionally, a secondary emission coefficient of the dielectric material was considered, equating to 0.02, while maintaining an average energy of 2.5 eV.

In our investigation, we delved into the intricate dynamics of surface dielectric barrier discharge (DBD) systems, particularly focusing on the effects of alternating current (AC) voltage [26]. Despite its inherent instability compared to direct current (DC), AC voltage presents unique opportunities for dynamic control in aerodynamic flow applications. By introducing temporal variations in the electric field, AC voltage influences the behavior of ions near the dielectric surface, consequently impacting airflow dynamics over aerodynamic profiles. While DC voltage offers a more consistent electric field, the fluctuating nature of AC voltage allows for dynamic flow control, presenting potential advantages in specific aerodynamic scenarios. Our research seeks to elucidate the intricate interplay between AC voltage, dielectric properties, and ionic motion, laying the groundwork for the development of advanced aerodynamic flow control strategies [29].

The selection of parameters and simulation inputs in our study is grounded in a comprehensive review of existing experimental and numerical works in the field. Drawing upon a wealth of prior research, we have carefully chosen the key variables to be investigated in our simulation model. These parameters have been identified based on their significant influence on the behavior of dielectric barrier discharges in oxygen-rich environments, as highlighted by previous studies.

By leveraging insights from both experimental observations and numerical simulations conducted by various researchers [26, 27, 30]. We aim to ensure that our simulation setup accurately reflects real-world conditions and facilitates meaningful comparisons with existing data. This iterative process of parameter selection and validation against experimental and numerical findings serves to enhance the robustness and reliability of our simulation results, ultimately contributing to a more comprehensive understanding of the phenomena under study.

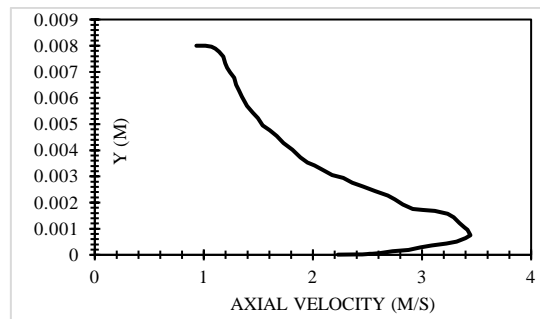


**Figure 4.** Profile of ion wind speed above an actuator located at  $x=12 \text{ mm}$  (from the exposed electrode) when subjected to a 10 kV alternating voltage at 250  $\mu\text{s}$

Indeed, our meticulous comparison and alignment with established research and experimental observations serve to underscore the credibility and accuracy of our model. The striking congruence observed between our findings and the established data not only validates the robustness of our simulation approach but also reinforces the reliability of our results within the realm of dielectric-material interaction under specific electrical conditions. This validation not only solidifies the confidence in our research outcomes but also contributes to the broader understanding of ion dynamics and their influence on aerodynamic flow control.

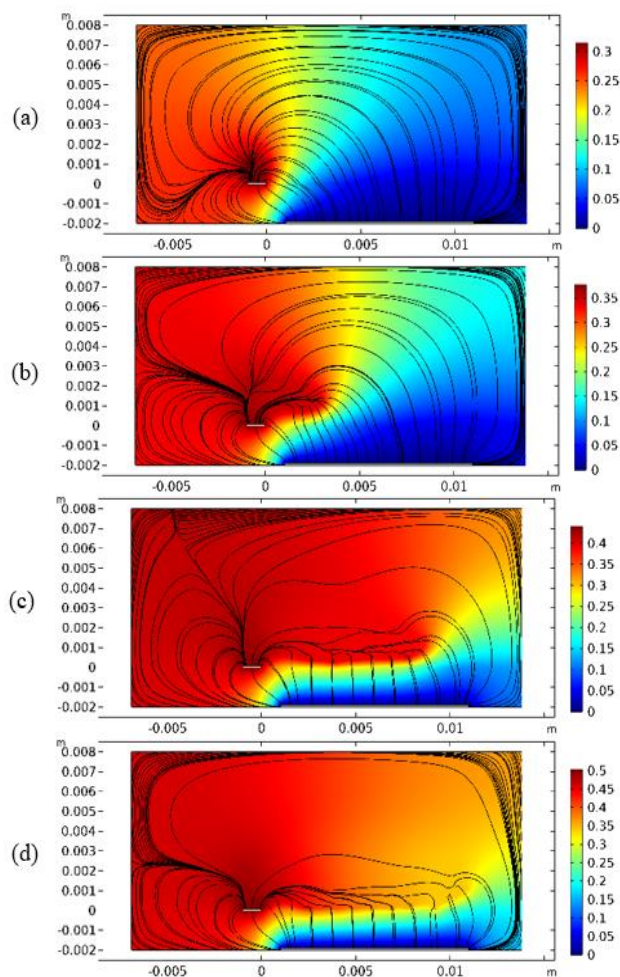


**Figure 5.** Spatial distribution of electric potential (kV) and electric field black lines at four different instants (a, b, c, and d) at 5, 6, 7, and 8 ns, respectively

In Figure 5, the electric field is described by the black lines and the voltages are described by the different colors. The covered electrode is the ground and the field is therefore always zero in the simulation. The electric field is stronger if the black lines (electric field lines) are close to each other and weaker if they are far from each other. Initially, the periodization electrons gain enough energy to make ionization collisions with neutral species in the gas (oxygen).

electric field allows ionization in this new region of space through the accumulation of surface charge. In effect, the electric field amplitude can be said to be higher near the edge of the exposed electrode and decreases as one moves longitudinally along the exposed dielectric surface. Therefore, the results suggest that the applied voltage plays a key role in the ionization and transfer of momentum in the DBD plasma actuator.

The results of this study show that the primary electron density has a significant impact on the formation and behavior of the plasma in the DBD plasma actuator. The simulation results demonstrate that the initial electron density of 108 electrons per cubic centimeter at time  $t=0$ , is sufficient to initiate the electric discharge. At the time  $t_1=10 \mu s$ , the breakdown is engaged, and the electron density rapidly increases to reach a maximum value of order  $4.5 \times 10^{20}$ , resulting in the formation of a plasma channel above the exposed dielectric surface.

This increase in electron density is due to the ionization collisions between the primary electrons and neutral species in the gas (oxygen). As the number of electrons in the plasma increases, more ionization collisions occur, leading to a positive feedback loop and a rapid increase in electron density.

The formation of a plasma channel above the exposed dielectric surface is an important result of this study. The plasma channel acts as a conduction channel, allowing the transfer of momentum between the charged species in the plasma and the neutral gas molecules. This transfer of momentum can be used to manipulate the airflow around wind turbine blades or aircraft wings, improving their performance.

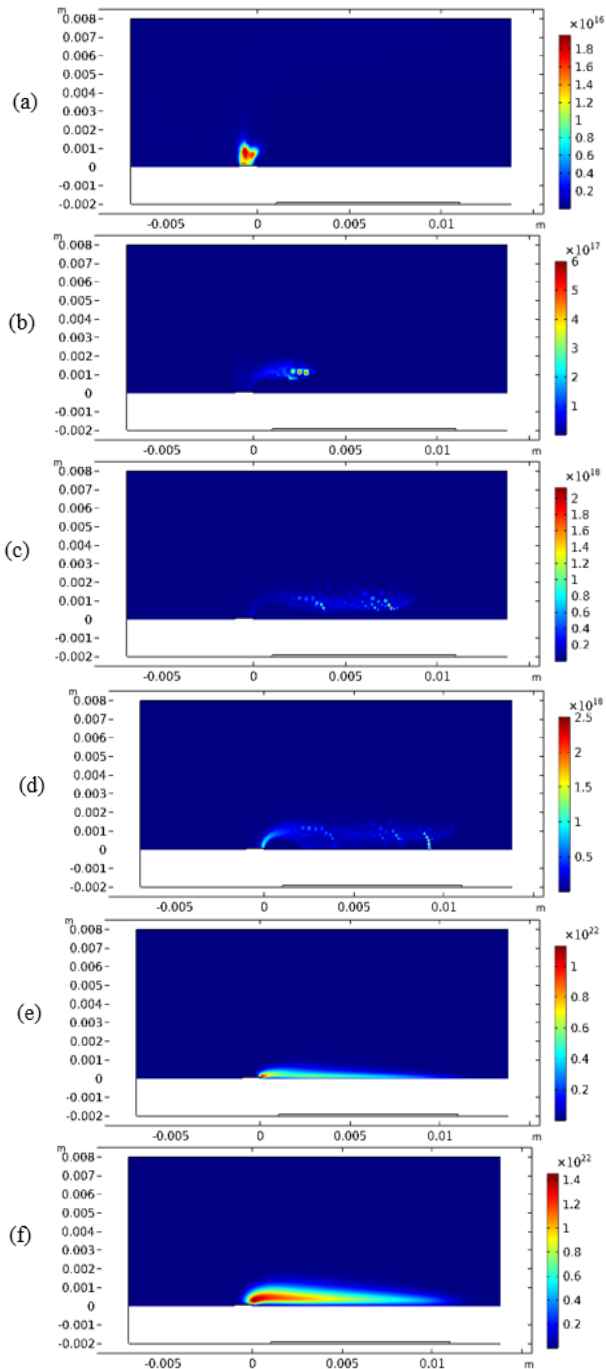


**Figure 6.** Spatial distribution of electron density ( $m^{-3}$ ) at six distinct time points (a, b, c, d, e and f) after 5, 6, 7, 8, 100 and 400 ns, correspondingly

In the positive half-cycle of the applied voltage, free electrons drift towards the high-voltage electrode and deposit on its surface, while positive ions are repelled from it. These results in an increase in the charge density of the space, which creates a conduction channel, thus increasing the electric potential and creating an electric field further away. This

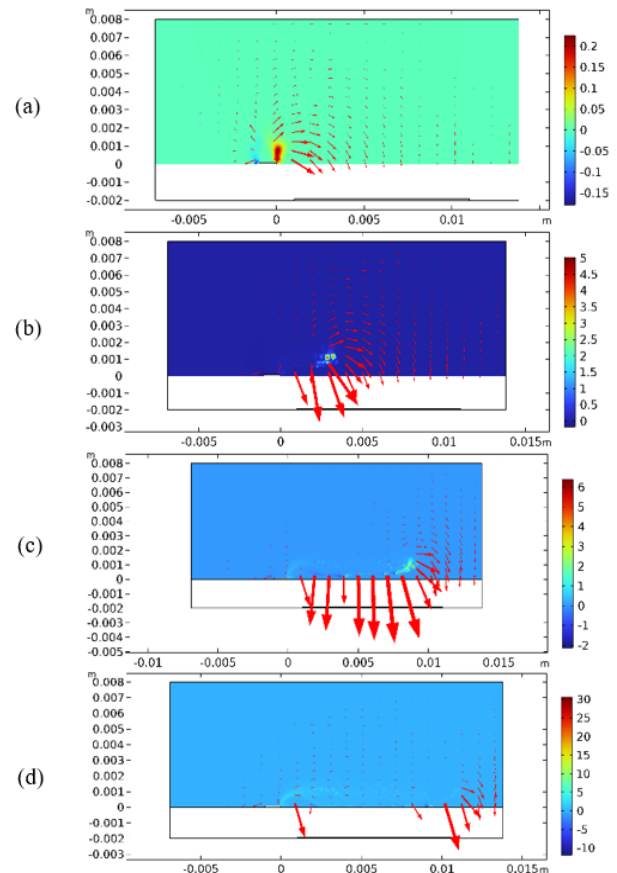


**Figure 7.** Spatial distribution of ion current density ( $A/m^2$ ) and velocity at different points in time (a, b, c and d) as a function of time (5, 6, 7 and 8 ns) with dielectric permittivity  $\epsilon_r=2.5$

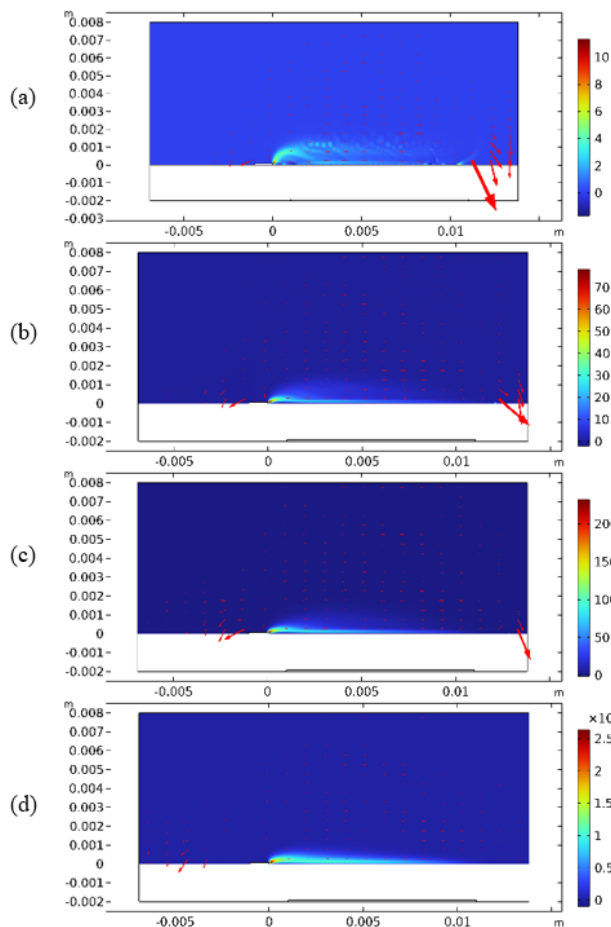


**Figure 8.** Spatial distribution of ion current density ( $A/m^2$ ) and velocity at different points in time (a, b, c and d) as a function of time (10, 15, 20 and 100 ns) with dielectric permittivity  $\epsilon_r=2.5$

The results discussed suggest that there are several factors contributing to the behavior of the electron density in the plasma Figure 6. At time  $t_2=6 \mu s$ , the electron density is directed tangentially to the dielectric surface, which is likely due to interactions with the oxygen plasma and the influence of the electric field. During the intervals  $t_3=7 \mu s$  and  $t_4=8 \mu s$ , there is an increase in electron density due to secondary electron emission from the dielectric material, as well as an augmentation of the applied voltage, reaching maximum values near the high-voltage electrode of  $1.1 \times 10^{22}$  at time  $t_5=100 \mu s$  and  $1.42 \times 10^{24}$  at time  $t_6 = 400 \mu s$ , respectively.

This secondary emission contributes to the ionization front and helps to produce a more significant electron avalanche. These results suggest that the behavior of the electron density in the plasma is complex and dependent on multiple factors, including plasma interactions with the dielectric surface, the influence of the electric field, and secondary electron emission. Understanding these factors is crucial for designing and optimizing plasma-based technologies and processes.

Figures 7 and 8 depict the spatial and temporal fluctuation of positive ion current density. The arrows showcase the velocity at the edge of the ionization wave propagation, particularly above the dielectric surface Figures 4 and 13. In this specific vicinity, Electrohydrodynamics (EHD) causes a charge accumulation leading to an increase in ionic density. One noteworthy finding is the increase in ion density from 0.2 to  $2.5 \times 10^4 A/m^2$ , with a significant speed, particularly near dielectric materials, as illustrated in Figures 7(b, c, and d).

Under the influence of Coulomb forces, charged particles in plasma gain kinetic energy. Electrons, which have a much higher density than positive ions, move at a faster rate, resulting in a greater frequency of collisions between electrons and neutrals compared to ions and neutrals. Although the mass discrepancy between electrons and ions is important, it is generally accepted that electrons play a significant role in transferring kinetic energy to neutrals. The discharge application on the dielectric surface creates an EHD (Electro Hydrodynamic) force on the adjacent gas at the oxygen-plasma interface, eliciting a tangential flow towards the dielectric.

Figure 9 illustrates the spatial variation of ion velocity at the precise instant  $t=250 \mu s$  along the horizontal axis, highlighting a significant decrease in ionic velocity as the distance from the high-voltage electrode increases. This phenomenon is characterized by a gradual reduction in the velocity of positive ions, ultimately reaching a zero value at a distance of 14 mm from the anode within the context of a dielectric barrier discharge device. This evolution is explained by the diminishing intensity of the electric field with distance, resulting in a decrease in ion acceleration, along with the impact of more frequent collisions with neutral particles and potential ion recombination events.

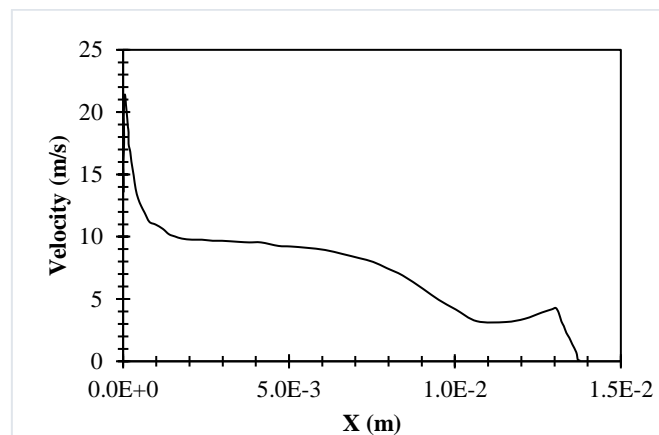


**Figure 9.** Visualisation of spatial changes in ion velocity at 250  $\mu s$ , corresponding to the first peak of applied voltage during the first half cycle along the horizontal axis

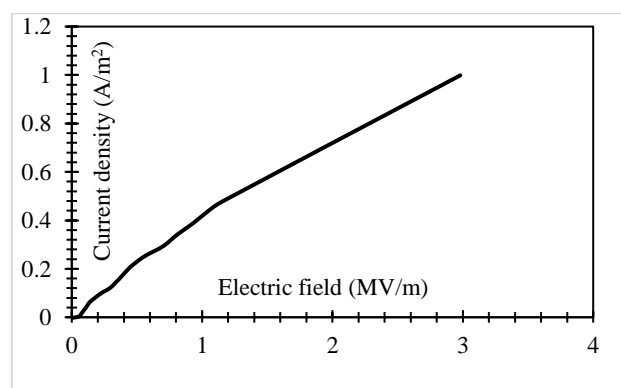


**Figure 10.** Correlation between electric field intensity and surface current density in plasma actuator instrument for ion acceleration

The decrease in positive ion velocity as distance from the high-voltage electrode increases can be explained by fundamental principles in plasma physics. The ions experience

a large acceleration near the electrode due to the intense electric field. Nevertheless, as they move farther away, the electric field weakens, resulting in a reduction in acceleration. Moreover, intensified interactions with neutral particles in the plasma area cause collisions and recombination processes, leading to a gradual reduction in ion velocity until it eventually reaches zero velocity at a specific distance from the electrode. Figure 10 demonstrates that the surface current density rises with an increase in the electric field norm magnitude, suggesting a direct link between the electric field intensity and surface current density. This correlation substantially contributes to the acceleration and ensuing conduct of ions within the plasma actuator instrument.

The variation of the ion velocity in a DBD plasma actuator as a function of the dielectric permittivity depends on several factors, such as the applied voltage, the frequency of the applied electric field, the gas composition, and the geometry of the actuator.

In general, the dielectric permittivity affects the electric field distribution in the plasma actuator and therefore the ionization rate and the ion drift velocity. A higher dielectric permittivity can lead to a stronger electric field in the plasma actuator, which can increase the ionization rate and the ion drift velocity. However, if the dielectric permittivity is too high, the electric field can become too localized and the discharge may not propagate over the entire surface of the actuator, leading to reduced ion velocity.

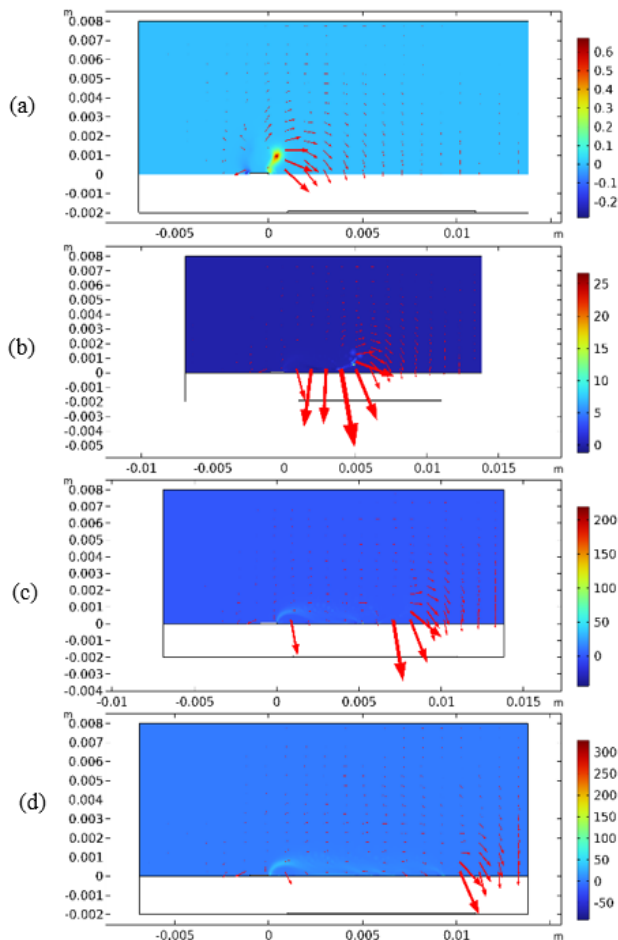


**Figure 11.** Spatial distribution of ion current density ( $A/m^2$ ) and velocity at different points in time (a, b, c and d) as a function of time (5 ,6, 7 and 8 ns) with dielectric permittivity  $\epsilon_r=5$

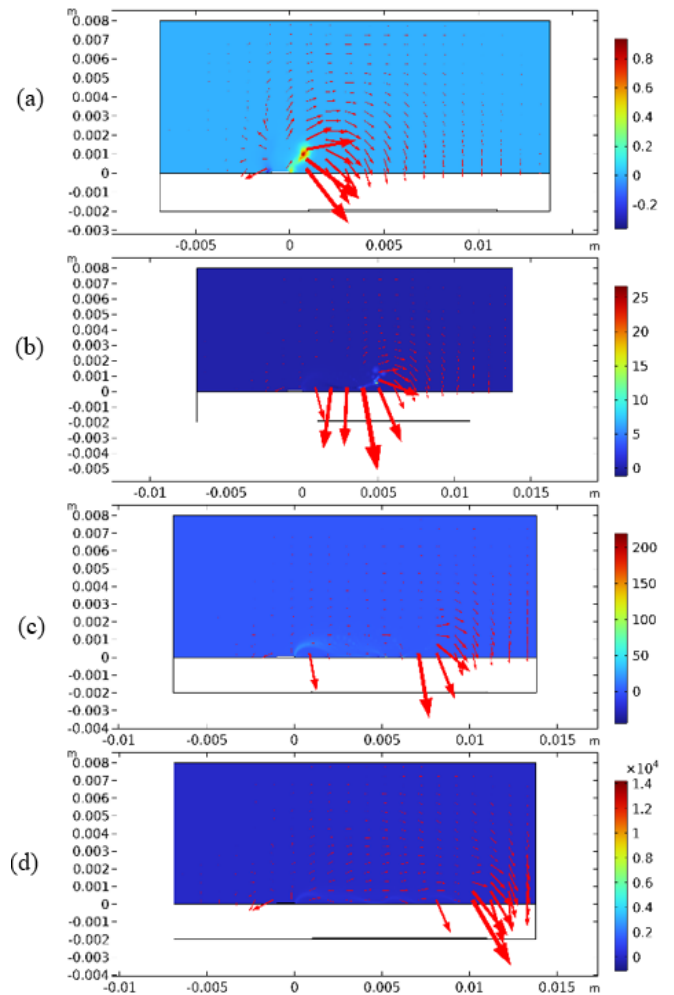


**Figure 12.** Spatial distribution of ion current density ( $A/m^2$ ) and velocity at different points in time (a, b, c and d) as a function of time (5, 6, 7 and 8 ns) with dielectric permittivity  $\epsilon_r=10$

Experimental studies have shown that increasing the dielectric permittivity of the dielectric barrier in a plasma actuator can increase the ion velocity and the thrust generated by the actuator. For example, in a study of a plasma actuator using helium gas and a dielectric barrier made of polyethylene terephthalate (PET) with varying thickness, it was found that increasing the thickness of the PET barrier (which corresponds to increasing the dielectric permittivity) increased the ion velocity and the thrust [31].

However, theoretical and numerical analyses have illuminated the complexity of this relationship, emphasizing that the impact of dielectric permittivity on ion velocity is contingent upon several additional factors. For example, a numerical study of a DBD plasma actuator using argon gas and a dielectric barrier made of quartz found that increasing the dielectric permittivity of the barrier decreased the ion velocity due to a reduction in the electric field strength and the ionization rate [32, 33].

In our simulation, as depicted in Figures 7, 8, 11, and 12, we observe a consistent increase in ion wind speed with higher dielectric permittivity. This is due to the increase in the electric field applied to the gas, which in turn increases with the dielectric permittivity. The higher the dielectric permittivity, the greater the electro hydrodynamic force. The EHD force is the force that acts on an ionized fluid in the presence of an

electric field. It is generated by the interaction between the electric charges and the electric field. In summary, the increase in dielectric permittivity leads to an increase in the EHD force, which increases the speed of the ion wind.

The dielectric permittivity of a plasma actuator can have a significant effect on ion velocity, but it is a complex issue that involves a variety of factors. The dielectric material used in the actuator can affect the electric field distribution, which, in turn, can alter the ion velocity. Additionally, the frequency and power of the electrical signal used to create the plasma can also affect the ion velocity.

The statement highlights the fact that the relationship between dielectric permittivity and ion velocity in a plasma actuator is not straightforward and involves several interdependent factors. Dielectric permittivity affects the distribution of electric fields within the plasma, which in turn influences the motion and behavior of charged species, including ions. However, the exact nature and extent of this influence depend on multiple factors, including the plasma actuator's design, the type of dielectric material used, and the operating conditions.

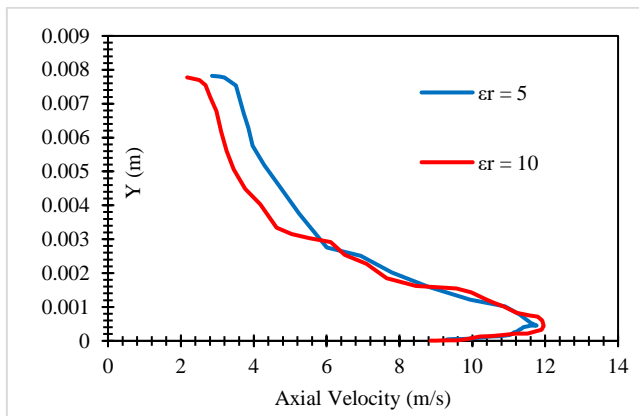


**Figure 13.** Profile of ion wind speed above an actuator located at  $x=12$  mm (from the exposed electrode) when subjected to a 10 kV alternating voltage at 250  $\mu$ s

For instance, the dielectric permittivity of the material can alter the strength and distribution of the electric fields, which affects the acceleration and deceleration of ions within the plasma. The geometry and composition of the plasma actuator can also impact the ion velocity as well as the dielectric breakdown and discharge characteristics. The ion velocity is further influenced by the plasma density and temperature, which are in turn influenced by various external factors such as the applied electric field and gas flow rates.

Figure 13 illustrates the correlation between ion velocity and vertical position at a distance of 12 mm from the exposed high-voltage electrode (anode) at precisely  $t=250$   $\mu$ s. This correlation is assessed for varying dielectric permittivity values, differentiated by red ( $\epsilon_r=10$ ) and blue ( $\epsilon_r=5$ ) curves. The findings denote a substantial trend: a noticeable surge in ionic velocity is witnessed alongside the rise in dielectric permittivity. The correlation between ionic velocity and dielectric permittivity indicates a direct and notable influence of the latter on the kinetics of ions in the examined medium. The fluctuations in dielectric permittivity seem to affect the mobility of ions at that particular moment, leading to different values of ionic velocity at particular permittivity levels.

Numerical simulations assessed the influence of dielectric permittivity on ion dynamics in a plasma actuator, which

demonstrated a clear correlation between ion velocity and permittivity. The findings verified the model's reliability against experimental data and uncovered the intricate impact of factors including electron density, energy application, and actuator geometry on plasma dynamics.

## 5. CONCLUSIONS

In conclusion, this study has provided valuable insights into the characteristics and dynamics of plasma actuators, with a particular focus on the influence of dielectric permittivity on ion velocity. Through meticulous simulations, we have identified parameters affecting these devices and assessed their optimization potential for aerodynamic and energy applications. Our findings reveal significant spatial and temporal variations in the electric field, electron and ion densities, and ion velocity, underscoring the crucial importance of dielectric permittivity in plasma dynamics. Moreover, the correlation of our results with empirical data attests to the accuracy of our model, thus enhancing its reliability and validity. Figures 5 to 12 present a detailed analysis of plasma-dielectric interactions and their impact on ion dynamics induced by electric fields. Particularly, Figure 13 highlights the direct relationship between ion velocity and dielectric permittivity, emphasizing the critical significance of this factor in the design and optimization of plasma actuators. These results offer promising prospects for enhancing plasma actuators, especially in the realms of aerodynamics and energy. Importantly, the application of these findings in flow control for wind turbines holds considerable potential. By manipulating ion dynamics near the surface of wind turbine blades, plasma actuators can effectively mitigate flow separation, delay stall onset, and enhance overall aerodynamic efficiency. However, it is crucial to acknowledge that further research is warranted to fully explore plasma-dielectric interactions and leverage the full potential of these emerging technologies. In summary, this study contributes to a deeper understanding of plasma actuators and opens new avenues for their development and application in various fields. We hope that our findings will serve as a foundation for future research endeavors and inspire innovation in this exciting and evolving domain.

## REFERENCES

- [1] Tehrani, D.S., Abdizadeh, G.R., Noori, S. (2022). Numerical modeling of dielectric barrier discharge actuators based on the properties of low-frequency plasmons. *Scientific Reports*, 12(1): 10378. <https://doi.org/10.1038/s41598-022-14370-z>
- [2] Singh, K.P., Roy, S. (2008). Force approximation for a plasma actuator operating in atmospheric air. *Journal of Applied Physics*, 103(1): 013305. <https://doi.org/10.1063/1.2827484>
- [3] Singh, K.P., Roy, S. (2007). Modeling plasma actuators with air chemistry for effective flow control. *Journal of Applied Physics*, 101(12): 123308. <https://doi.org/10.1063/1.2749467>
- [4] Singh, K.P., Roy, S., Gaitonde, D. (2006). Modeling of dielectric barrier discharge plasma actuator with atmospheric air chemistry. In 37th AIAA Plasmadynamics and Lasers Conference, San Francisco, USA, pp. 3381. <https://doi.org/10.2514/6.2006-3381>

- [5] Singh, K.P., Roy, S. (2005). Simulation of an asymmetric single dielectric barrier plasma actuator. *Journal of Applied Physics*, 98(8): 083303. <https://doi.org/10.1063/1.2103415>
- [6] Shaygani, A., Adamiak, K. (2023). Mean model of the dielectric barrier discharge plasma actuator including photoionization. *Journal of Physics D: Applied Physics*, 56(5): 055203. <https://doi.org/10.1088/1361-6463/aca43>
- [7] Nishida, H., Abe, T. (2010). Numerical analysis for plasma dynamics in SDBD plasma actuator. In 41st Plasmadynamics and Lasers Conference, Chicago, USA, pp. 4634. <https://doi.org/10.2514/6.2010-4634>
- [8] Likhanskii, A., Shneider, M., Miles, R., Macheret, S. (2011). Numerical investigation of pulsed-driven DBD plasma actuator. In APS Annual Gaseous Electronics Meeting Abstracts, pp. TF1-006.
- [9] Nesaecian, M., Homaeinezhad, M.R. (2023). Analytical input-output modelling of surface dielectric barrier discharge plasma actuator. *Journal of Physics D: Applied Physics*, 56: 465204. <https://doi.org/10.1088/1361-6463/acefe0>
- [10] Neretti, G., Cristofolini, A., Borghi, C.A., Gurioli, A., Pertile, R. (2012). Experimental results in DBD plasma actuators for air flow control. *IEEE Transactions on Plasma Science*, 40(6): 1678-1687. <https://doi.org/10.1109/TPS.2012.2191801>
- [11] Lilley, A.J., Roy, S., Michels, L., Roy, S. (2022). Performance recovery of plasma actuators in wet conditions. *Journal of Physics D: Applied Physics*, 55(15): 155201. <https://doi.org/10.1088/1361-6463/ac472d>
- [12] Khalaf, T.H., Ghayb, D.H. (2022). Computational study of charge density produced in N<sub>2</sub>: H<sub>2</sub> plasma actuator. *Trends in Sciences*, 19(9): 3476-3476. <https://doi.org/10.48048/tis.2022.3476>
- [13] Font, G., Enloe, L., McLaughlin, T., Orlov, D. (2007). Plasma discharge characteristics and experimentally determined boundary conditions for a plasma actuator. In 45th AIAA Aerospace Sciences Meeting and Exhibit, Reno, USA, pp. 188. <https://doi.org/10.2514/6.2007-188>
- [14] Zhao, G., Li, Y., Liang, H., Han, M., Wu, Y. (2015). Flow separation control on swept wing with nanosecond pulse driven DBD plasma actuators. *Chinese Journal of Aeronautics*, 28(2): 368-376. <https://doi.org/10.1016/j.cja.2014.12.036>
- [15] Kwan, P.W., Huang, X. (2019). A pedagogical study of aerodynamic feedback control by dielectric barrier discharge plasma. *IEEE Transactions on Industrial Electronics*, 67(1): 451-460. <https://doi.org/10.1109/TIE.2019.2897514>
- [16] Fujii, K. (2018). Three flow features behind the flow control authority of DBD plasma actuator: Result of high-fidelity simulations and the related experiments. *Applied Sciences*, 8(4): 546. <https://doi.org/10.3390/app8040546>
- [17] Houser, N.M., Gimeno, L., Hanson, R.E., Goldhawk, T., Simpson, T., Lavoie, P. (2013). Microfabrication of dielectric barrier discharge plasma actuators for flow control. *Sensors and Actuators A: Physical*, 201: 101-104. <https://doi.org/10.1016/j.sna.2013.06.005>
- [18] Corke, T.C., Enloe, C.L., Wilkinson, S.P. (2010). Dielectric barrier discharge plasma actuators for flow control. *Annual Review of Fluid Mechanics*, 42: 505-529. <https://doi.org/10.1146/annurev-fluid-121108-145550>
- [19] Chetan, M. (2023). Active aerodynamic load control for wind turbines. Mayank Chetan. <https://www.mayankchetan.com/project/plasmaproject/>, accessed on Mar. 13, 2023.
- [20] Dong, B., Hong, D., Pouvesle, J.M., Boucinha, V., Weber, R., Leroy, A. (2008). Study of a DBD plasma actuator dedicated to airflow separation control. In 2008 IEEE 35th International Conference on Plasma Science, Karlsruhe, Germany, pp. 1-1. <https://doi.org/10.1109/PLASMA.2008.4590781>
- [21] Faranosov, G., Bychkov, O.P., Kopiev, V., Kopiev, V.A., Moralev, I., Kazansky, P. (2019). Plasma-based active closed-loop control of instability waves in unexcited turbulent jet. Part 1. Free jet. In 25th AIAA/CEAS Aeroacoustics Conference, Delft, The Netherlands. <https://doi.org/10.2514/6.2019-2557>
- [22] Shaygani, A., Adamiak, K. (2023). Mean model of the dielectric barrier discharge plasma actuator including photoionization. *Journal of Physics D: Applied Physics*, 56(5): 055203. <https://doi.org/10.1088/1361-6463/aca43>
- [23] Balcon, N. (2007). Atmospheric pressure Radio Frequency discharges, diagnostic and numerical modeling. Doctoral dissertation, Université Paul Sabatier-Toulouse III; Australian National University. <https://theses.hal.science/tel-00211176>
- [24] Ouali, M., Seddaoui, N., Lagmich, Y. (2022). Comparative study between different macroscopic approximations for cold plasma modeling. *Open Access Library Journal*, 9(11): 1-13. <https://doi.org/10.4236/oalib.1109497>
- [25] Shaygani, A., Adamiak, K. (2023). Mean model of the dielectric barrier discharge plasma actuator including photoionization. *Journal of Physics D: Applied Physics*, 56(5): 055203. <https://doi.org/10.1088/1361-6463/aca43>
- [26] Bai, L., Lin, G., Peterson, G.P., Wen, D. (2011). Modeling and analysis of supercritical startup of a cryogenic loop heat pipe. *Journal of Heat and Mass Transfer*, 133(12): 121501. <https://doi.org/10.1115/1.4004595>
- [27] Moreau, E. (2007). Airflow control by non-thermal plasma actuators. *Journal of Physics D: Applied Physics*, 40(3), 605-636. <https://doi.org/10.1088/0022-3727/40/3/S01>
- [28] Ouali, M., Lagmich, Y. (2024). Enhanced plasma jet generation through numerical integration and dielectric influence analysis. *AIP Advances*, 14(1): 015318. <https://doi.org/10.1063/5.0187175>
- [29] Sato, S., Enokido, T., Ohnishi, N. (2021). Fabrication of a multi-stage plasma synthetic jet actuator using printed electronics. *AIP Advances*, 11: 045105. <https://doi.org/10.1063/5.0047709>
- [30] Corke, T.C., Thomas, F.O. (2018). Active and passive turbulent boundary-layer drag reduction. *AIAA Journal*, 56(10): 3835-3847. <https://doi.org/10.2514/1.J056949>
- [31] Lagmich, Y., Callegari, T., Pitchford, L.C., Boeuf, J.P. (2008). Model description of surface dielectric barrier discharges for flow control. *Journal of Physics D: Applied Physics*, 41(9): 095205. <https://doi.org/10.1088/0022-3727/41/9/095205>
- [32] Palombo, M., Malagoli, A., Pani, M., Bernini, C., Manfrinetti, P., Palenzona, A., Putti, M. (2015).

Exploring the feasibility of Fe (Se, Te) conductors by ex-situ powder-in-tube method. *Journal of Applied Physics*, 117(21): 213903. <https://doi.org/10.1063/1.4921902>

- [33] Mestiri, R., Hadaji, R., Ben Nasrallah, S. (2010). An experimental study of a plasma actuator in absence of free airflow: Ionic wind velocity profile. *Physics of Plasmas*, 17(8): 083503. <https://doi.org/10.1063/1.3474924>

## NOMENCLATURE

V	electric potential, V
I	electric current, A
E	electric field, V
q	electric charge, C
AC	alternating current
DC	direct current
n	electron density, m <sup>-3</sup>
m	electron mass

u	electron drift velocity
T	temperature, K
P	diffusion coefficient
D	diffusion coefficient
S	source term that depends on the ionization

## Greek symbols

$\Gamma$	particle flux, m <sup>2</sup> . s <sup>-1</sup>
$\mu$	particle mobility, m <sup>2</sup> . V <sup>-1</sup> s <sup>-1</sup>
$\varepsilon$	mean electron energy, V
$\varepsilon_r$	dielectric relative permittivity

## Subscripts

DBD	dielectric barrier discharge
EHD	electro hydrodynamic
LEA	local energy approximation
LFA	local field approximation
nf	local thermal equilibrium